



OPEN

## KRT7 promotes pancreatic cancer metastasis by remodeling the extracellular matrix niche through FGF2-fibroblast crosstalk

Yuting Jiang<sup>1,2,4,5</sup>, Chengyu Liao<sup>1,3,4,5</sup>✉, Jianlin Lai<sup>1,3,4,5</sup>, Yunyi Peng<sup>1</sup>, Qilin Chen<sup>1</sup> & Xiaoling Zheng<sup>1,2,4</sup>✉

Pancreatic ductal adenocarcinoma (PDAC) is a devastating cancer with a dismal prognosis due to distant metastasis. Through an analysis of large RNA sequencing and proteomics datasets, we found that high KRT7 expression in PDAC patients was correlated with liver metastasis and poor survival. A functional investigation revealed that the overexpression of KRT7 promoted liver metastasis but did not affect tumor cell proliferation *in vivo* or *in vitro*. Analysis of scRNA-Seq data from 24 PDAC samples revealed a negative correlation between KRT7 expression in PDAC cells and cancer-associated fibroblast (CAF) infiltration, and this was further confirmed in orthotopic tumor model mice injected with KRT7-overexpressing PDAC cells, which led the development of a prometastatic niche with reduced ECM deposition. Mechanistically, KRT7 in PDAC cells promoted the secretion of FGF2, which inhibited CAF proliferation and ECM-related gene transcription through the Wnt/β-catenin pathway. Moreover, targeting FGF2 decreased liver metastasis *in vivo*. Our study revealed that KRT7 promotes PDAC liver metastasis by remodeling the extracellular matrix niche through FGF2-fibroblast crosstalk and provides a promising strategy for preventing PDAC liver metastasis.

**Keywords** Pancreatic ductal adenocarcinoma, Metastasis, Extracellular matrix, Cancer-associated fibroblasts, Fibroblasts

Pancreatic ductal adenocarcinoma (PDAC) is one of the most aggressive malignancies; the primary cause of death is distant metastasis, predominantly through hematogenous routes, and the liver is the most common site of such metastases<sup>1,2</sup>. Distant PDAC metastasis involves multiple steps, including the detachment of tumor cells from the primary site, penetration through the extracellular matrix (ECM), intravasation, extravasation, and ultimately, colonization and growth at distant sites<sup>3</sup>. Among these steps, the traversal of tumor cells through the ECM is a pivotal, rate-limiting process<sup>4</sup>. The ECM, which is mainly composed of collagens, serves as a physiological barrier, hindering the crucial step of tumor cell intravasation<sup>5</sup>. Therefore, further investigation into the behavior of PDAC cells within the ECM has the potential to yield new insights into the mechanisms underlying the distant metastasis of PDAC.

ECM deposition and degradation in the tumor microenvironment (TME) are intricately linked to tumor immunology, and ECM generation is predominantly mediated by cancer-associated fibroblasts (CAFs)<sup>6,7</sup>. CAFs respond to paracrine signals, modulating the ECM to facilitate metastasis via the secretion transforming growth factor beta (TGFβ), chemokine (C-X-C motif) ligand 12 (CXCL12), matrix metalloproteinase 9 (MMP9) and interleukin-6 (IL-6), which contribute to ECM remodeling or degradation, thereby supporting tumor cell metastasis<sup>6,8,9</sup>. Furthermore, tumor-derived exosomes activate Kruppel-like factor 4 (KLF4) in CAFs, leading to cellular detachment and subsequent deposition of fibronectin, establishing a prometastatic niche conducive to hematogenous spread<sup>10</sup>. Despite the critical role of the ECM in shaping the prometastatic niche, research specifically addressing the ECM-supported metastatic niche in PDAC is still limited. Therefore, a more in-depth analysis of the interplay between PDAC and CAFs during this process would help elucidate the changes in the ECM, consequently providing evidence for how these interactions facilitate metastasis. This knowledge holds

<sup>1</sup>Shengli Clinical Medical College of Fujian Medical University, Fuzhou 350001, China. <sup>2</sup>Department of Digestive Endoscopy, Fujian Provincial Hospital, No. 134 East Street, Fuzhou 350001, China. <sup>3</sup>Department of Hepatobiliary Pancreatic Surgery, Fujian Provincial Hospital, No.134 East Street, Fuzhou 350001, China. <sup>4</sup>Fuzhou University Affiliated Provincial Hospital, Fuzhou 350001, China. <sup>5</sup>Yuting Jiang, Chengyu Liao and Jianlin Lai contributed equally to this work. ✉email: 455930732@qq.com; fzhengxl@163.com

promise for the development of novel therapeutic strategies targeting ECM remodeling and CAF activation to prevent the distant metastasis of PDAC.

Keratin 7 (KRT7), a member of the type II keratin family, is a major component of the intermediate filament cytoskeleton<sup>11</sup>. It is closely associated with tumor progression and metastasis<sup>11</sup>. During epithelial–mesenchymal transition (EMT) in ovarian cancer cells, downregulation of E-cadherin and claudins promotes cellular motility, whereas KRT7 expression remains stable or even increases<sup>11,12</sup>. An et al. demonstrated that activation of the TGF-β/Smad2/3 pathway by KRT7 is key for inducing EMT in ovarian cancer; matrix metalloproteinases (MMP2 and MMP9), key enzymes involved in ECM degradation, are also closely related to KRT7 activity<sup>11</sup>. These observations suggest that KRT7 may play a role in degrading the ECM, which is intimately linked to its invasive properties. Moreover, via its antisense molecule KRT7-AS, KRT7 facilitates p65 phosphorylation and nuclear translocation, indicating significant potential for transcriptional activation<sup>13</sup>. Nonetheless, the interplay between KRT7 and CAFs in PDAC remains unclear. Given its potential for transcriptional activation, KRT7 may promote certain extracellular signals to modulate CAFs, thereby altering the ECM and facilitating metastasis. However, this hypothesis has yet to be proven.

Here, for the first time, we identified KRT7 as an important molecule in the distant metastasis of PDAC through multiomics analysis of RNA-Seq and proteomic data for PDAC samples. KRT7 promotes the metastasis of PDAC in a TME-dependent manner, inhibits CAF invasion and ECM generation through FGF2 signaling, and thus induces the formation of a migration-conducive niche with decreased deposition of ECM to support the distant metastasis of pancreatic cancer. This study reveals that targeting FGF2-fibroblast crosstalk in PDAC patients with high KRT7 expression is a promising treatment strategy.

## Methods

### Cell culture and transfection

Human PDAC cells (PANC1; AsPC1) were obtained from the American Type Culture Collection (ATCC; Manassas, VA, USA) and were cultured in standard medium supplemented with heat-inactivated FBS and antibiotics (50 U/mL penicillin and 50 mg/L streptomycin) according to the manufacturer's recommendations in a humidified atmosphere at 37 °C and 5% CO<sub>2</sub>. PA02 cells were purchased from Pricella Life Science & Technology Co., Ltd., and cultured with complete culture medium for PA02 cells (Pricella Life Science & Technology Co., Ltd., CM-0675) at 37 °C and 5% CO<sub>2</sub>. Human pancreatic CAFs were purchased from SAIOS (Wuhan) and cultured in DMEM supplemented with 10% FBS at 37 °C and 5% CO<sub>2</sub>. All the cell lines were confirmed to be free of mycoplasma and were authenticated by short tandem repeat analysis. KRT7-overexpressing lentiviruses and control empty-vector (EV)-overexpressing lentiviruses were purchased from GeneChem (Shanghai, China). Lentivirus transduction was performed according to the instructions provided by GeneChem (Shanghai, China).

### 3D tumor spheroid growth assay

First, tumor cell monolayers were washed with PBS, and then, cell dissociation enzyme (Gibco 25200072) was added to obtain a single-cell suspension. The cells were then counted with a hemacytometer and diluted to a concentration of 0.5 to 2 × 10<sup>3</sup> cells/mL to determine the optimal cell density for each cell line. Then, the cell suspension was transferred to a sterile container, and a multichannel pipette was used to add 200 μL of the suspension to each well of a circular bottom ultralow adhesion (ULA) 96-well plates (1500 cells/well). The plates were transferred to an incubator (37 °C, 5% CO<sub>2</sub>, 95% humidity) to allow growth. Images were obtained via microscopy to measure changes in sphere size over a continuous period of 96 h<sup>14,15</sup>.

### 3D tumor spheroid migration assay

As mentioned above, 3D-tumor spheroids were allowed to form for 4 days, and their formation was visually confirmed before the migration assays began. Then, the spheroids were gently transferred to a migration 96-well plate precoated with gelatin. Complete growth medium was added. Then, the spheres were allowed to adhere to the coating surface for 60 min, and images were taken from 0 to 48 h. The relative migration of the initial tumor sphere was quantified<sup>15</sup>.

### CCK-8 assay

Cell viability was analyzed via Cell Counting Kit-8 (CCK-8; Beyotime, Shanghai, China) assays according to the manufacturer's protocols. The cells were seeded and cultured at a density of 5 × 10<sup>3</sup>/well in 100 μL of medium in 96-well plates. After 24 h, 10 μL of CCK-8 reagent was added to each well, and the cells were then cultured for 2 h. All the experiments were performed in triplicate. The absorbance was analyzed at 450 nm with a microplate reader (Bio-Rad, Hercules, CA, USA), and wells without cells were used as blanks. The proliferation of the cells is expressed as the absorbance.

### In vivo indirect coculture system

To coculture PDAC cells and CAFs, six-well Transwell plates with 0.4-μm porous polycarbonate membranes (Corning, USA) were used. PDAC cells were seeded in the upper chamber, and CAFs were seeded in the lower chamber. The cells were cocultured for 24 h and then used for subsequent experiments.

### Orthotopic model

BALB/c nude mice and C57BL/6 mice (4–6 weeks old) were purchased from Shanghai SLAC Laboratory Animal Co., Ltd. (Shanghai, China). Age-matched littermates were also used in this study. Both male and female mice were used. All the mice were housed under specific pathogen-free (SPF) conditions at the Anburui BD Laboratory (Fuzhou, China). The sample size was estimated using power analysis for group comparisons by one-way ANOVA<sup>16</sup>: for two-group comparisons, the minimum sample size in each group was 10/2 + 1 = 6, and the

maximum sample size in each group was  $20/2 + 1 = 11$ . The acceptable sample size in each group was 6 to 11. The number of mice in each experiment is indicated in the corresponding figure legend. All animals were handled in strict accordance with the Principles for the Utilization and Care of Vertebrate Animals and the Guide for the Care and Use of Laboratory Animals. For the animal studies, the ears of the mice were marked before the animals were divided into groups by an independent investigator, and the experimental and control animals were housed separately. At the end of the animal experiments, the mice were euthanized by cervical dislocation. The investigators were aware of the group allocations at the different stages of the experiment (during allocation, the experiment itself, outcome assessment, and data analysis).

To prepare an orthotopic tumor models: PANC1, ASPC1 or PA02 cells ( $10^6$  cells per mouse) transfected with an empty vector or KRT7-overexpressing vector were implanted into the pancreas after anesthesia. Six weeks later, the tumors and liver were harvested after the mice were euthanized for further analysis. The tumor volume was determined each week after injection; specifically, electronic calipers were used to measure the length (L) and width (W):  $0.52 \times L \times W \times W$ . The maximum size of the tumors did not exceed 2 cm according to the guidelines of our institution's ethical board. The early termination criteria were as follows: (1) a maximum cumulative tumor diameter of 2.0 cm; (2) the presence of a tumor that impeded eating, urination, defecation, or ambulation; and (3) very poor body condition. The animal experiments were reported following ARRIVE guidelines.

### ELISA

Cells culture supernatants were collected and centrifuged at  $1000 \times g$  for 10 min. The concentrations of secreted TGFB1 and FGF2 in the supernatants were measured with a human TGFB1 ELISA kit and a human FGF2 ELISA kit according to the manufacturer's protocol (Enzyme-linked Biotechnology, Shanghai, China).

### In vitro ECM assembly and invasion transwell assay

ECM assembly was induced as described in a previous study<sup>17</sup>. Transwell inserts were coated with gelatin solution (0.2% in PBS) at  $37^\circ C$ . The inserts were then washed twice with PBS prior to the addition of glutaraldehyde (1% in PBS) for cross-linking. After the plates were washed twice with PBS, 1 mol/L glycine solution was added to the plates to stop the crosslinking reaction for 20 min at room temperature. The inserts were then washed once with PBS. PBS supplemented with 1× penicillin–streptomycin was added to each well. The inserts were finally sealed with parafilm and stored at  $4^\circ C$  for a maximum of 3 days prior to cell seeding. The gelatin-coated inserts were retrieved and washed twice with PBS. Serum-containing DMEM/RPMI was added to the wells, and the plates were incubated at  $37^\circ C$  for at least 1 h for warming and equilibration of the gelatin layer. Then, CAFs together with different PDAC cells (1:1,  $3 \times 10^4$ ) were seeded on the precoated Transwell inserts and allowed to attach to the bottom of the wells overnight. The next morning, the medium was aspirated, and the wells were washed once with PBS prior to the addition of ECM assembly medium (DMEM/RPMI supplemented with 0.2% FBS, 1× penicillin–streptomycin and 50 µg/mL freshly prepared sodium ascorbic acid; 500 µL per well), which was replaced every other day. ECM assembly was induced in 5%  $CO_2$  and 3%  $O_2$  6 days after seeding of the CAFs and PDAC cells. To preserve the ECM, the wells were first washed twice with PBS. Cell lysis solution (0.5% Triton and 20 mmol/L NH4OH in PBS) was added to the wells, and the plates were subsequently incubated for 5 to 8 min at  $37^\circ C$ . PBS was then added to the wells to dilute the lysis solution. The inserts were then sealed and stored at  $4^\circ C$  overnight. The next morning, the plates were washed three times with PBS for additional Transwell assays. For the next invasion Transwell assay,  $3.0 \times 10^4$  wild-type PANC1 cells or ASPC1 cells were suspended in FBS-free medium and plated in the upper chamber of the Transwell plate. The lower chamber was filled with complete medium containing 10% FBS. After 24 h, the migrated cells on the lower surface of the insert were fixed with methanol for 20 min and stained with 0.5% crystal violet solution for 20 min for quantification.

### Picosirius red staining

For ECM analysis, tumor samples were stained with a Picosirius Red Stain Kit. The samples were fixed in 4% paraformaldehyde at room temperature for 15 min, and routine dehydration and embedding were performed. The samples were sliced at a thickness of 6–7 µm, dewaxed in water via conventional methods, and stained with Sirius Red staining solution for 1 h. The slices were rinsed quickly with running water to remove the staining solution on the surface. The samples were subjected to conventional dehydration, clearing and sealing with neutral gum<sup>18</sup>. The samples were observed under a regular optical microscope, and images were taken for quantification via ImageJ software.

### Immunofluorescence

The samples were fixed in 4% paraformaldehyde at room temperature for 15 min, permeabilized with 0.2% Triton X-100 for 10 min, and then blocked with 5% BSA at room temperature for 1 h. The slices were incubated overnight with primary antibodies at  $4^\circ C$  and then incubated with fluorescent secondary antibodies at room temperature for 1 h. The samples were mounted after being stained with diamidino-2-phenylindole (DAPI).

### Data acquisition and analysis

The gene expression data, including those from The Cancer Genome Atlas (TCGA), GSE71729 and GSE151580, were obtained from the UCSC Xena (<https://xena.ucsc.edu/>) and GEO (GEO, <https://www.ncbi.nlm.nih.gov/ge/o/>) databases. The proteomics data were obtained from processed files from a study by Shen et al.<sup>19</sup>, which were analyzed using the R package 'limma' and subsequently adjusted using the Benjamini–Hochberg method. Two-sided *p* values were calculated. Online data analysis tools (<https://www.xiantaozi.com/>) were used to identify differentially expressed genes (DEGs) via the DESeq2 method, and the following thresholds were used: adjusted *p* value (Benjamini–Hochberg method)  $< 0.05$  and  $|\log_2 FC| < 1$ .

## Statistical analysis

GraphPad Prism 9.0 and SPSS 26.0 were used for the statistical analyses. Between-group differences in the data were assessed via Student's t test. The Mann–Whitney U test was used to compare nonnormally distributed data. Overall survival (OS) and recurrence-free survival (RFS) were assessed via the Kaplan–Meier method and compared via the log-rank test. The  $\chi^2$  test and Mann–Whitney U test were used to evaluate the associations between KRT7 levels and clinicopathological parameters in patients with PDAC. Representative data are shown as the means  $\pm$  SEMs.  $p < 0.05$ ,  $^{**}p < 0.01$ , and  $^{***}p < 0.001$  indicated statistical significance, and a  $p$  value of  $\geq 0.05$  indicated that the difference was not significant (ns).

## Results

### KRT7 is a key molecule for distant liver metastasis of PDAC

To analyze the heterogeneity of PDAC metastasis, we first analyzed the RNA-Seq data of a large cohort of PDAC patients (GSE71729). First, we identified 460 DEGs between PDAC tissues and adjacent tissues from the GSE71729 dataset (DEGs-GSE71729)<sup>20</sup> (Fig. 1A). Among these genes, 285 were upregulated, and 175 were downregulated (Fig. 1A). Moreover, we identified DEGs between PDAC tissues and adjacent tissues from the TCGA-PDAC dataset (DEGs-TCGA). Among these genes, 8730 were upregulated, and 480 were downregulated (Fig. 1B). We subsequently analyzed PDAC data from the GSE151580 dataset, which consisted of paired primary tumor data and corresponding distant liver metastasis data, and 3384 downregulated genes and 2421 downregulated genes were identified<sup>21</sup> (Fig. 1C). By intersecting the DEGs from the GSE71729, TCGA, and GSE151580 datasets, we identified 296 common DEGs as potential key genes for distant liver metastasis of PDAC (Fig. 1D).

Considering that genes often exert their functions through their protein products, we further analyzed a large-scale proteomic dataset comprising data from PDAC patients (NM proteomics), with information on 4787 proteins<sup>19</sup> (Fig. 1E). Initially, we identified the differentially expressed proteins (DEPs) within this dataset; specifically, there were 1213 upregulated and 864 downregulated proteins in tumor tissue compared with adjacent normal tissue (Fig. 1E). Notably, the changes in the expression (upregulation or downregulation) of 66 proteins coincided with changes in the expression of previously identified DEGs (Fig. 1E). These findings suggest that these 66 molecules are candidate factors potentially influencing distant liver metastasis in patients with pancreatic cancer, indicating that they may be important factors in the metastatic process.

Furthermore, we analyzed the association of survival outcomes with these 66 candidate molecules. Using the online GEPIA2 database<sup>22</sup>, we rigorously categorized PDAC samples into high-expression and low-expression groups on the basis of the median expression values of these genes. We identified a set of genes that could stratify patients into groups with differential overall survival (OS-median) and another set that could stratify patients into groups with differential disease-free survival (DFS-median) (Fig. 1F). We also grouped patients into high- and low-expression groups according to quartiles and identified genes that could stratify patients into groups with differences in overall survival (OS-quartile) and disease-free survival (DFS-quartile) with these cutoffs (Fig. 1F). Among the 66 candidate molecules, only one, KRT7, could be used to stratify patients according to survival, with both median and quartile cutoff values for high vs. low expression (Fig. 1F). The groups exhibited significant differences in survival according to data from both the KM plotter database and the TCGA database (Fig. 1G–I).

We subsequently investigated the expression of KRT7 via the GEPIA2 database and found that KRT7 was more highly expressed in tumor tissue than in normal tissue and was more highly expressed in patients with more advanced-stage PDAC than in those with early-stage PDAC (Fig. 1J,K). According to an analysis of our in-house clinical PDAC samples, high KRT7 expression was associated with an increased incidence of liver metastasis and lymph node metastasis, higher CA199 levels and a more advanced AJCC stage (Supplementary Table 1).

Next, we investigated the specific expression of KRT7 in the TME. Consistent with its upregulation in tumor tissue in the GEPIA2 database, we confirmed that it was upregulated in tumor tissues in our in-house PDAC cohort (Fig. 2A)<sup>22</sup>. Using scRNA-Seq data from 24 PDAC samples from the CancerSCEM database, we found that KRT7 was highly expressed mainly in PDAC cells, as indicated by its high expression in the malignant cell population identified by the UMAP plot and its relatively low expression in other immune cells (Fig. 2B)<sup>23</sup>. Furthermore, immunohistochemical (IHC) staining data for KRT7 from the Human Protein Atlas confirmed this finding (Fig. 2C). This evidence suggested that KRT7 is expressed specifically in tumor cells rather than in other cells of the TME. Accordingly, KRT7 was identified as a potential essential molecule for distant liver metastasis of PDAC.

### KRT7 promotes PDAC liver metastasis in vivo

Next, we examined the effects of KRT7 on PDAC liver metastasis. First, we overexpressed KRT7 in the PDAC cell lines PANC1 and ASPC1 through lentiviral transduction (Fig. 2D,E). After confirming the overexpression efficiency of KRT7 through Western blot analysis, we used BALB/c nude mice to construct an orthotopic model by injecting  $10^6$  cells into the pancreas. After six weeks, we sacrificed the mice and harvested the tumors, which revealed no significant differences in primary tumor size or tumor weight (Fig. 2F,G). However, the mice injected with KRT7-overexpressing cells had a greater incidence of liver metastasis (6/8; 5/8) than did the mice injected with empty vector (EV)-transfected cells (1/8; 1/8) (Fig. 2H). Moreover, in mice with liver metastasis, the metastatic burden was greater in those bearing KRT7-overexpressing cells than in those bearing EV-transfected cells (Fig. 2I,J). Similar results were also observed in C57BL/6 mice injected with PA02 cells transfected with the EV or overexpressing KRT7 (Fig. 2K–M). These results revealed the liver metastasis-promoting effect of KRT7.

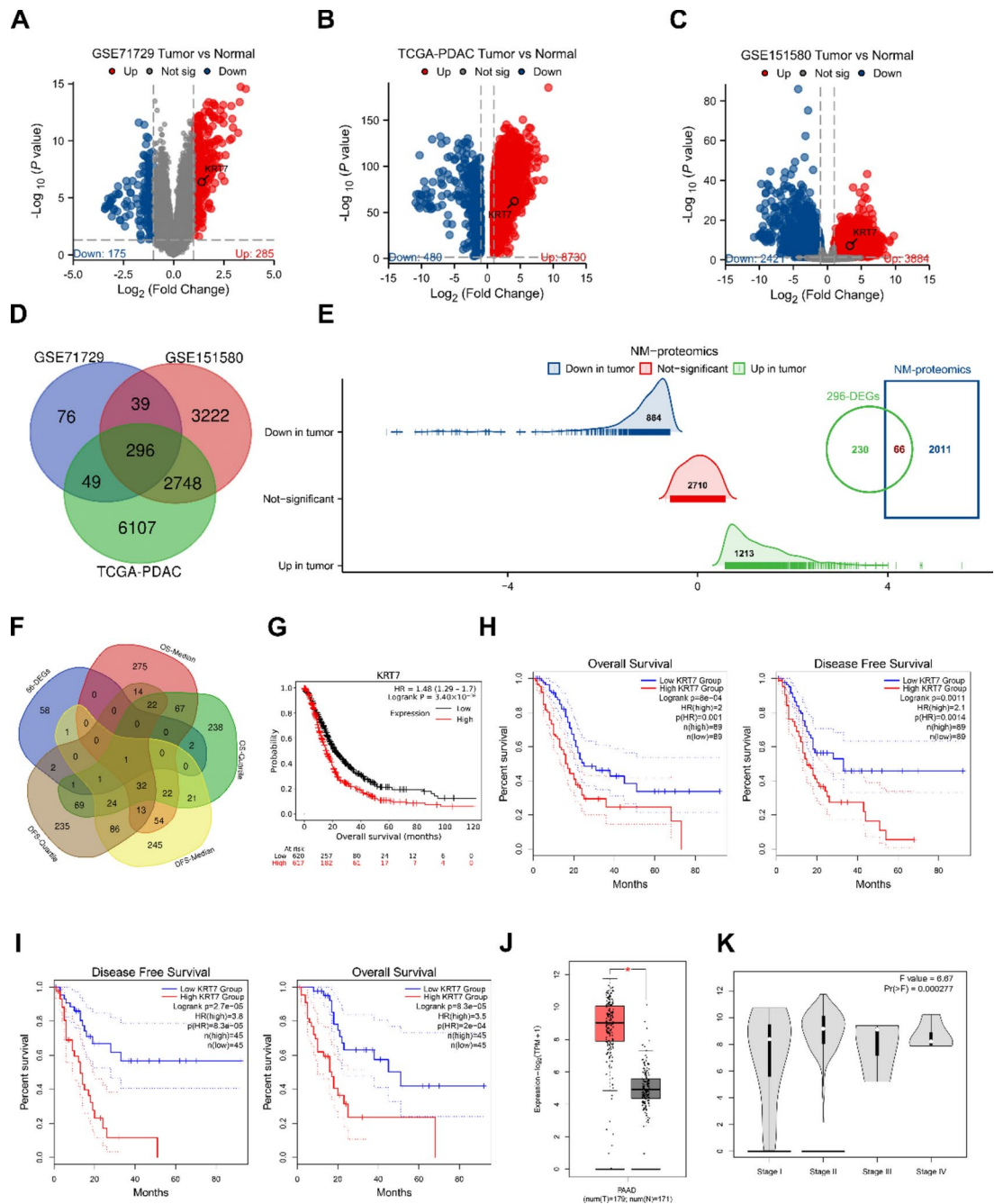
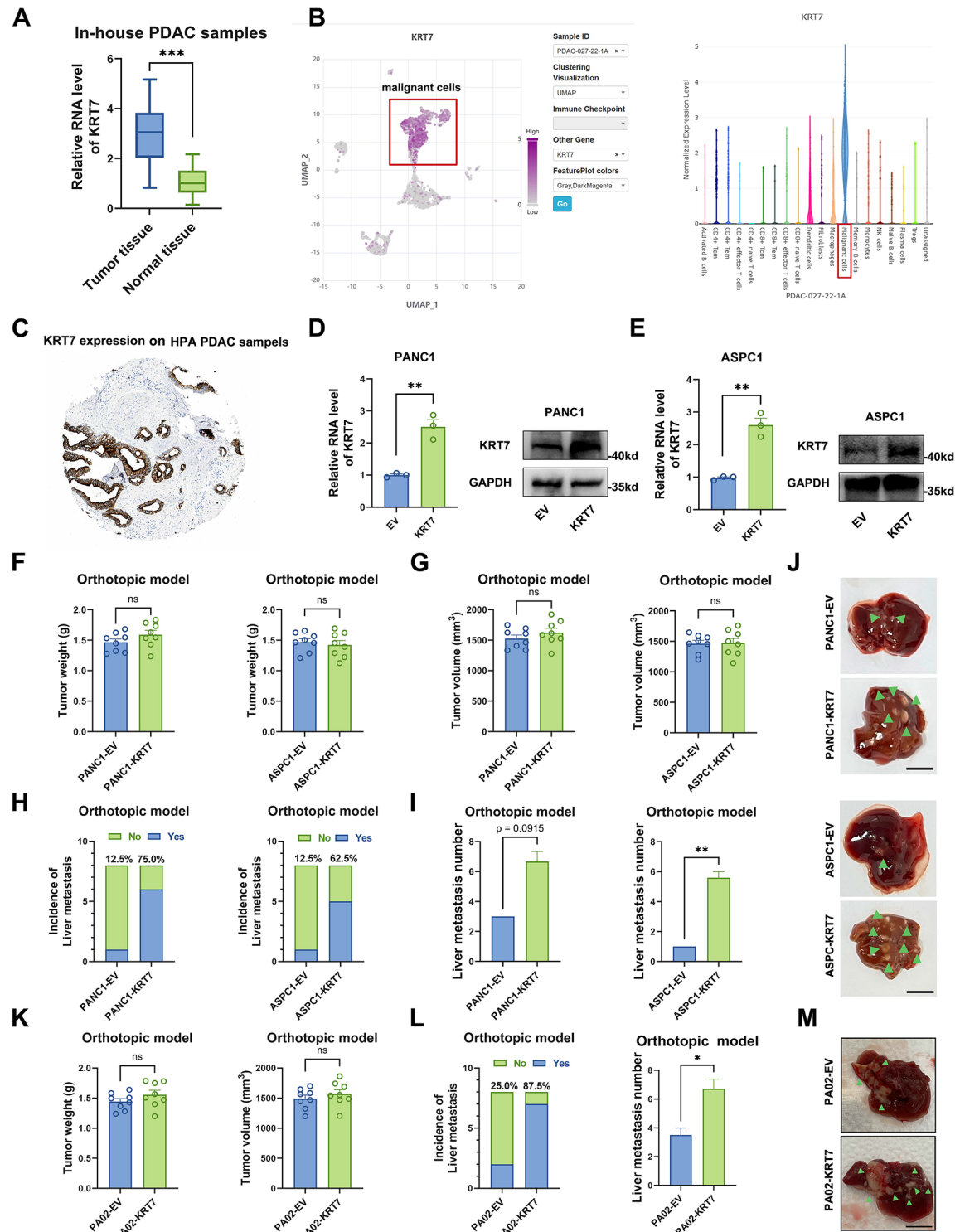


**Fig. 1.** Identification of KRT7 as a differentially expressed gene. (A) Volcano plot ( $|\log_2\text{FC}| > 1$ ,  $P \text{ value} < 0.05$ ) of the GSE71729 data. (B) Volcano plot ( $|\log_2\text{FC}| > 1$ ,  $P \text{ value} < 0.05$ ) of the TCGA-PDAC data. (C) Volcano plot ( $|\log_2\text{FC}| > 1$ ,  $P \text{ value} < 0.05$ ) of the GSE151580 data. (D) Venn diagram of the overlapping DEGs among the GSE71729, TCGA and GSE151580 dataset. (E) Differential mountain maps of PDAC samples according to proteomics. (F) Venn diagram of KRT7 overexpression data. (G) OS probability curve of patients stratified by KRT7 expression according to data from the KM plotter database. (H) OS and DFS curves of patients stratified by the median KRT7 expression level according to data from the GEPIA2 database. (I) OS and DFS curves of patients stratified by KRT7 expression quartiles according to data from the GEPIA2 database. (J) The expression of KRT7 in tumor and normal tissues according to data from the GEPIA2 database. (K) The expression of KRT7 in patients with PDAC of different AJCC stages according to data from the GEPIA2 database.

## KRT7 promotes PDAC liver metastasis in a TME-dependent manner

To further determine how KRT7 promotes PDAC liver metastasis, we next investigated the impacts of KRT7 on PDAC cells through functional experiments. First, we used a 3D culture technique to generate 3D tumor spheroids. Interestingly, the growth of KRT7-overexpressing tumor spheroids did not differ from that of EV-



transfected tumor spheroids (Fig. 3A,B). Additionally, Western blot analysis of proliferating cell nuclear antigen (PCNA) and the CCK-8 assay confirmed that KRT7-overexpressing PDAC cells and EV-transfected PDAC cells exhibited similar proliferation abilities (Fig. 3C,D). These results and the similar tumor weights and volumes *in vivo* indicated that KRT7 does not promote PDAC proliferation.

Next, we investigated the difference in metastatic ability between KRT7-overexpressing and EV-transfected tumor spheroids. In the 3D tumor spheroid-based migration assay, we did not observe a distinct increase in migration ability (Fig. 3E,F). These *in vitro* results suggested that the liver metastasis-promoting effects of KRT7 may involve other steps of the metastasis process rather than the initial steps of increased metastatic ability in PDAC cells. This shifted our attention to the TME in this context.

**Fig. 2.** The expression and liver metastasis-promoting effect of KRT7 in PDAC. (A) The RNA level of KRT7 in PDAC tissue and normal tissue samples from our in-house cohort. (B) Representative UMAP plot and a corresponding plot showing the expression of KRT7 in different cell types according to data from the online PDAC scRNA-Seq CancerSCEM database. (C) Representative images of IHC staining for KRT7 in samples from the Human Protein Atlas database. (D) The RNA and protein levels of KRT7 after transfection of EV or a KRT7 overexpression vector into PANC1 cells. (E) The RNA and protein levels of KRT7 after transfection of EV or a KRT7 overexpression vector into ASPC1 cells. (F) Primary tumor weights and volumes in BALB/c nude orthotopic mice injected with PANC1 cells transfected with the EV or KRT7 overexpression vector. The mice were euthanized 6 weeks after injection; n = 8 mice per group. (G) Primary tumor weights and volumes in the BALB/c nude orthotopic mice injected with ASPC1 cells transfected with the EV or KRT7 overexpression vector. The mice were euthanized 6 weeks after injection; n = 8 mice per group. (H) Incidence of liver metastases in BALB/c nude orthotopic mice injected with PANC1 and ASPC1 cells transfected with the EV or KRT7 overexpression vector; n = 8 mice per group. The mice were euthanized at 4 weeks after injection. (I) Quantification of liver metastatic nodes in the BALB/c nude orthotopic mouse model. (J) Representative images of gross morphology of metastatic liver tumors in the BALB/c nude orthotopic mouse model. (K–M) Primary tumor weights, tumor volumes, incidence of liver metastases, number of liver metastasis nodes and representative gross morphology of metastatic liver tumors in C57BL/6 orthotopic mice injected with  $10^6$  PA02 cells transfected with the EV and KRT7 overexpression vector; n = 8 mice per group. The mice were euthanized 6 weeks after injection.

### KRT7 is associated with less fibroblast infiltration and a less dense ECM niche

To determine the TME features of KRT7, we analyzed the cellular components of 24 PDAC samples via scRNA-Seq data derived from the CancerSCEM database (Fig. 4A)<sup>23</sup>. The percentages of CD4+ T cells, CD8+ T cells, and NK cells in the KRT7<sup>high</sup> PDAC samples (samples 04, 08, 09, 14, 17, 20, 21, and 22) did not significantly differ from those in the KRT7<sup>low</sup> PDAC samples (Fig. 4A). Interestingly, we detected increased fibroblast infiltration in the KRT7<sup>low</sup> PDAC samples compared with the KRT7<sup>high</sup> PDAC samples (samples 04, 08, 09, 14, 17, 20, 21, and 22) (Fig. 4A). To further confirm the negative correlation between KRT7 expression and fibroblast infiltration, we examined fibroblast infiltration in tissue samples from our in-house PDAC cohort through immunofluorescence. Consistent with the findings reported above, the KRT7<sup>high</sup> PDAC samples presented decreased fibroblast infiltration, as reflected by decreased α-SMA staining intensity (Fig. 4B).

CAFs remodel the TME by secreting ECM-degrading enzymes or by generating the ECM. Here, we observed a decrease in the abundance of infiltrating CAFs, which shifted our attention to the subsequent impacts of CAFs on the ECM. Thus, we used a picrosirius staining assay to assess the ECM content. A lower ECM content was also observed in the KRT7<sup>high</sup> PDAC samples (Fig. 4C), which suggested a metastasis-conducive niche.

### KRT7 promotes metastasis-conducive ECM niche formation by inhibiting CAF infiltration through FGF2

Next, we investigated the crosstalk between PDAC cells and CAFs to determine the mechanism underlying the decrease in CAF infiltration and subsequent formation of a metastasis-conducive ECM niche. Tumor cells can secrete various cytokines, such as TGF-beta and FGF2, to affect CAFs<sup>24</sup>. Thus, we investigated the levels of these cytokines in KRT7-overexpressing cells and the corresponding supernatants. TGF-beta levels were not significantly different between KRT7-overexpressing cells or their supernatants compared with control cells and their supernatants (Fig. 5A).

In addition, FGF2 has been well documented to inhibit CAF proliferation and fibrotic gene expression, which could explain the decrease in CAF infiltration and subsequent decrease in ECM deposition caused by KRT7 overexpression<sup>24</sup>. We then examined the impact of KRT7 on FGF2 transcription, which revealed an obvious increase in FGF2 expression in both KRT7-overexpressing cells and their supernatants compared with the corresponding controls (Fig. 5B). Moreover, elevated FGF2 expression was also observed in tissue homogenates of orthotopic tumors overexpressing KRT7 (Fig. 5C). KRT7 has been reported to promote transcription<sup>13</sup>. Thus, we examined whether KRT promoted the transcription of FGF2. We detected increased transcription of FGF2 in KRT7-overexpressing PDAC cells (Fig. 5D). In addition, a positive correlation between KRT7 and FGF2 RNA expression was found according to data from the external PDAC ENCORI database (Fig. 5E). These results suggested that KRT7 promotes the secretion of FGF2, which may account for the decrease in CAF infiltration and subsequent decrease in ECM deposition caused by KRT7 overexpression.

We further investigated whether the increase in the amount of FGF2 secreted by KRT7-overexpressing cells was responsible for the increase in liver metastasis *in vivo*. We subsequently administered NSC12 (an FGF2 inhibitor, FGF2i), which acts as an extracellular FGF trap, binds FGF2 and interferes with its interaction with FGFR1, to BALB/c nude orthotopic model mice<sup>25</sup>. The decreases in CAF infiltration and ECM deposition were reversed by the addition of FGF2i (Fig. 5F,G). Moreover, we used a Transwell assay to evaluate the impacts of different cocultured CAF-secreted ECMs on the metastatic ability of PDAC cells. ECM produced by CAFs cocultured with KRT7-overexpressing PDAC cells resulted in aggressive metastasis of tumor cells, and the metastatic ability of these cells was rescued by ECM produced by CAFs cocultured with FGF2 knockdown KRT7-overexpressing PDAC cells (Fig. 5H). These results revealed that KRT7 promotes the transcription and secretion of FGF2 in PDAC cells, leading to metastasis-conducive ECM niche formation via inhibition of CAF infiltration.

The *in vitro* results suggested that FGF2 plays a key role in KRT7-induced CAF proliferation and ECM deposition. Then, we assessed the potential clinical value of FGF2i; FGF2i treatment also significantly attenuated

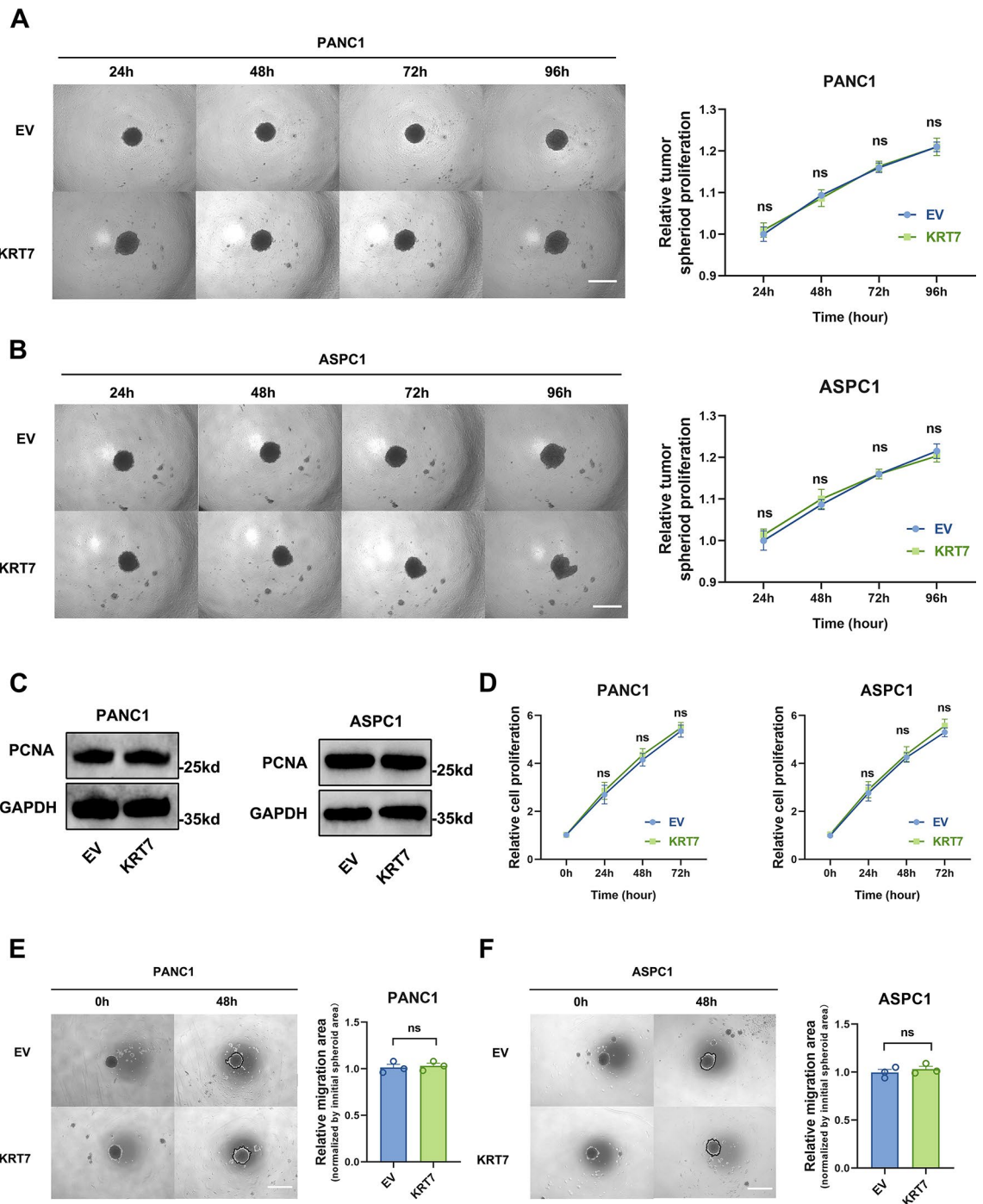


**Fig. 3.** The impacts of KRT7 on PDAC proliferation and metastasis in vitro. (A,B) Growth in the 3D tumor spheroid formation assay. A growth curve was generated by normalizing the tumor volume to the initial volume; n = 3 biologically independent samples; scale bar: 50  $\mu$ m. (C) Western blot analysis of PCNA levels in PDAC and ASPC1 cells. (D) CCK-8 assay. (E,F) Migration of tumor cells in the 3D tumor spheroid formation assay. The migration area is expressed relative to the initial tumor spheroid area during spheroid migration. The quantitative data are shown on the right; n = 3 biologically independent samples; scale bar = 50  $\mu$ m.

the increase in liver metastasis events caused by KRT7 overexpression in vivo (Fig. 5I,J). Moreover, the primary tumor weights remained stable (Fig. 5K). During FGF2i treatment, body weight loss was not observed in the mice (Fig. 5L). These findings suggested that FGF2i treatment is a promising intervention for preventing liver metastasis in KRT7<sup>high</sup> PDAC patients.

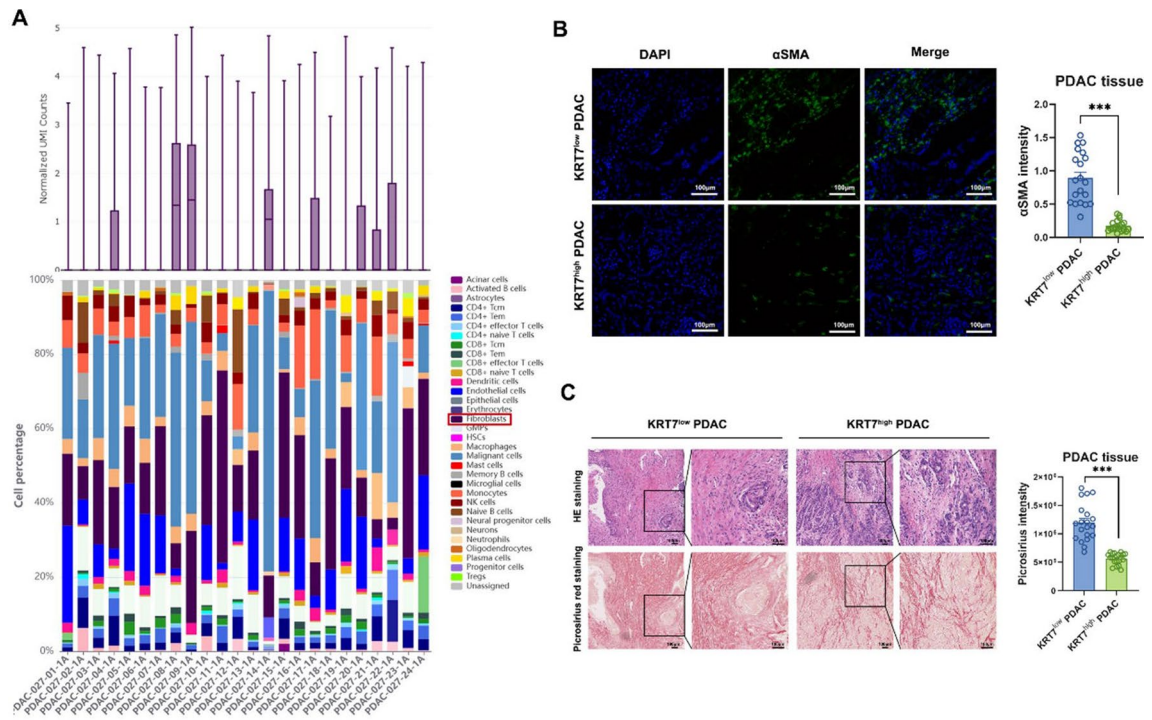


**Fig. 4.** KRT7 inhibits CAF infiltration and ECM deposition in PDAC. (A) Plot of KRT7 expression in PDAC cells and the percentage of immune cells in the corresponding sample according to data for 24 samples from the online PDAC scRNA-Seq CancerSCEM database. (B) Representative images and graph of  $\alpha$ -SMA staining in KRT7<sup>high</sup> and KRT7<sup>low</sup> PDAC tissue samples from our in-house cohort ( $n=20$  each group); scale bar: 100  $\mu$ m. (C) Representative picrosirius-stained images and a graph of picrosirius staining in KRT7<sup>high</sup> and KRT7<sup>low</sup> PDAC tissue samples from our in-house cohort ( $n=20$  each group); scale bar: 100  $\mu$ m.

## FGF2 inhibits CAF proliferation and the transcription of ECM-related genes through the Wnt- $\beta$ -catenin signaling pathway

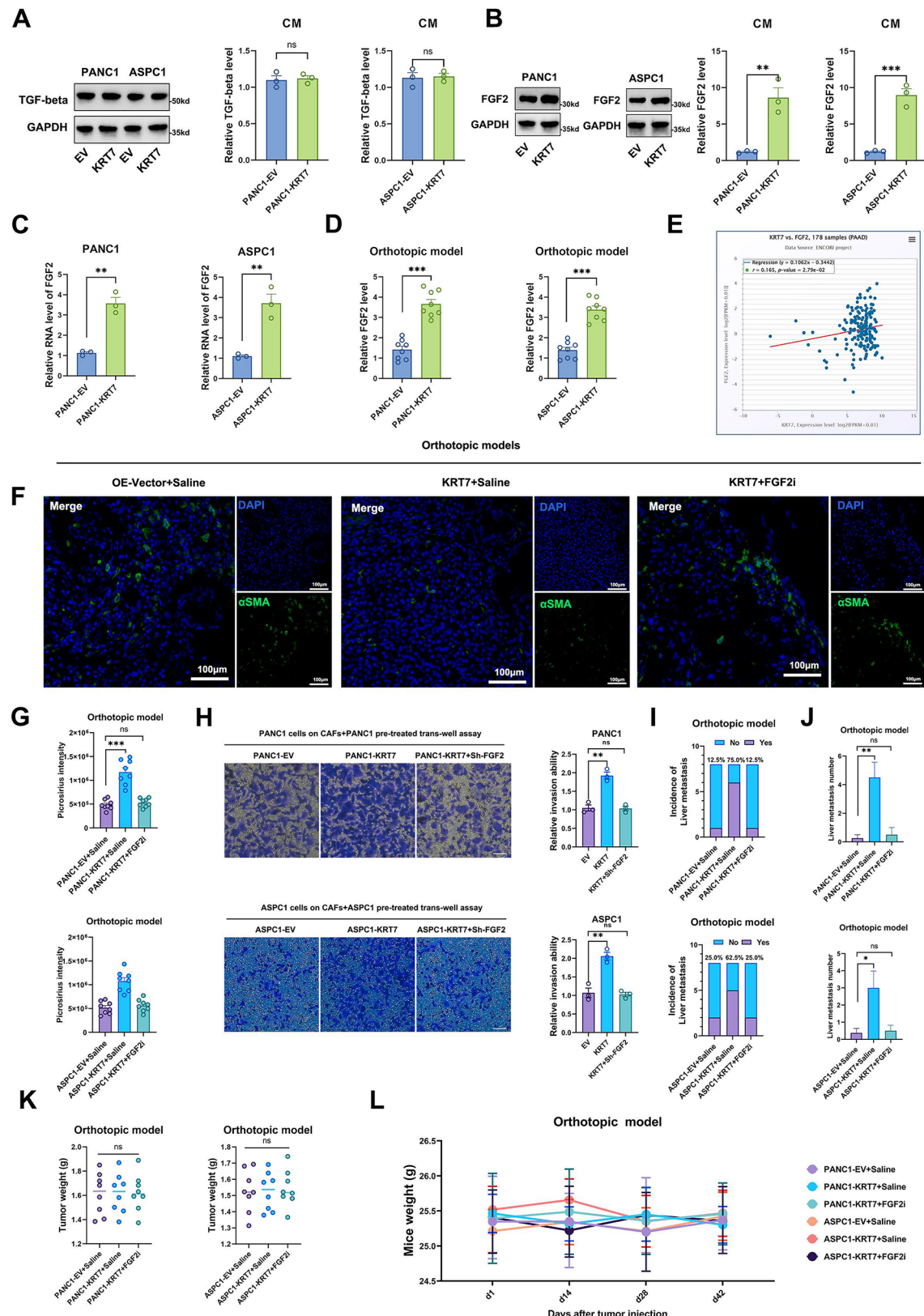
Next, we investigated the mechanism by which FGF2 shapes the metastasis-conducive ECM niche by inhibiting CAF infiltration. By using an *in vitro* indirect coculture system consisting of CAFs and PDAC cells, we examined the impacts of FGF2 on CAFs (Fig. 6A). To inhibit CAF infiltration, we first examined the changes in the proliferative ability of CAFs cocultured with KRT7-overexpressing tumor cells exposed to high FGF2 levels. CAFs cocultured with KRT7-overexpressing tumor cells exhibited decreased proliferative ability, as indicated by a decrease in PCNA expression, suggesting that the proliferative potential of CAFs was inhibited by FGF2 (Fig. 6B,C). Moreover, no changes in FGFR1 expression in CAFs were observed, excluding the possibility that decreased FGF2 receptor expression results from decreased FGFR1 expression.

Considering that the Wnt- $\beta$ -catenin pathway is the main downstream pathway of FGFR1<sup>26</sup> that potentially regulates the proliferative ability of CAFs, we detected decreased Wnt- $\beta$ -catenin pathway activity in CAFs cocultured with KRT7-overexpressing PDAC cells (Fig. 6B,C). To confirm this hypothesis, we next investigated whether a Wnt- $\beta$ -catenin signaling pathway agonist (SKL2001) could abolish the decrease in PCNA levels caused by FGF2<sup>27,28</sup>. SKL2001 rescued the decrease in PCNA expression in CAFs cocultured with KRT7-overexpressing tumor cells. These findings suggested that KRT7-overexpressing PDAC cells secrete more FGF2, which inhibits CAF proliferation by inhibiting the Wnt- $\beta$ -catenin pathway through FGFR1, thus decreasing CAF infiltration.

Next, we assessed the ability of CAFs in the coculture system to produce ECM by measuring the expression of ECM production-related genes, including *Acta2*, *Col1a1*, *Ctgf*, *Col3a1*, *Thbs1*, *Serprinh1*, *Sparc*, *Fn1* and *Tnc*, in CAFs<sup>24</sup>. These genes were markedly downregulated in CAFs cocultured with KRT7-overexpressing PDAC cells (Fig. 6D,E)<sup>29</sup>. These effects were reversed by treatment with FGF2i or SKL2001 (Fig. 6D,E)<sup>25,28</sup>. Additionally, the levels of the corresponding proteins, including αSMA, CTGF, COL3A1, THBS1, HSP47 and SPARC, were measured via Western blot analysis (Fig. 6F,G). The findings suggest that FGF2 derived from KRT7-overexpressing PDAC cells inhibits the Wnt-β-catenin pathway through FGFR1 to decrease the proliferation and transcription of ECM-producing genes in CAFs, thus leading to the formation of a metastasis-conducive niche with a less dense ECM.

## Discussion

The TME plays a pivotal role in facilitating pancreatic cancer metastasis through multiple steps<sup>3,30</sup>. Here, for the first time, we identified a crucial molecule for pancreatic cancer liver metastasis, KRT7, via multiomics data analysis employing stringent identification criteria. This study is the first to highlight the paramount impact of KRT7 on the prometastatic niche in PDAC and reveal the key regulatory function of FGF2 in modulating CAFs,



thereby reducing ECM deposition. We propose a promising strategy for inhibiting metastasis by targeting FGF2, offering novel insights into the mechanisms underlying distant metastasis in pancreatic cancer and suggesting new therapeutic approaches.

KRT7 was first identified as an important molecule affecting distant liver metastasis in pancreatic cancer patients. In contrast to most previous studies on prognostic molecules, we used both RNA-Seq and proteomic data to study changes not only at the RNA level but also at the protein expression level<sup>31</sup>. In addition, we used medians and interquartile ranges to identify differences in survival among patients treated with KRT7, reducing

**Fig. 5.** KRT7 promotes metastasis-conducive ECM niche formation by inhibiting CAF infiltration through FGF2. (A) Western blot analysis of TGF-beta levels in PANC1 cells and analysis of TGF-beta levels in the corresponding culture medium by ELISA. (B) Western blot analysis of FGF2 levels in PANC-1 cells and analysis of TGF-beta levels in the corresponding culture medium by ELISA. (C) The RNA level of FGF2 in PANC1 and ASPC1 cells. (D) Analysis of FGF2 levels in primary tumor tissue homogenates from BALB/c nude orthotopic model mice by ELISA. (E) Correlation analysis between KRT7 RNA levels and FGF2 RNA levels according to data from the online ENCORI PDAC dataset. (F,G) Representative images of  $\alpha$ -SMA staining and picrosirius staining of primary tumors from BALB/c nude orthotopic model mice that received different treatments (saline treatment or FGF2 inhibitor treatment (NSC12, 2.5 mg/kg, iv. 3x/week)); n = 8 mice per group. The mice were sacrificed 6 weeks after injection. (H) ECM assembly in an in vitro Transwell invasion assay; scale bar: 50  $\mu$ m. (I-K) Incidence of liver metastasis, number of liver metastasis nodes and tumor weight in BALB/c nude orthotopic tumor model mice that received different treatments (saline treatment or FGF2 inhibitor treatment (NSC12, 2.5 mg/kg, iv. 3x/week)); n = 8 mice per group. The mice were sacrificed 6 weeks after injection. (L) Body weights of BALB/c nude orthotopic tumor model mice that received different treatments (saline treatment or FGF2 inhibitor treatment (NSC12, 2.5 mg/kg, iv. 3x/week)).

grouping bias by using a single median expression value as the cutoff value. In addition, we analyzed a large set of RNA-Seq data from Western countries and proteomic data from China, which also reflects the universality of KRT7 as a biomarker for PDAC liver metastasis.

KRT7 was previously reported to directly facilitate the progression of colorectal and ovarian cancers<sup>11,32,33</sup>. Our investigations of PDAC using both two-dimensional (2D) and three-dimensional (3D) culture models confirmed that KRT7 does not directly influence the proliferative capacity of pancreatic cancer cells. Similarly, *in vivo*, KRT7 was found to not affect the proliferation of primary tumor lesions. Instead, we discovered that it promoted liver metastasis in PDAC by fostering the development of a prometastatic niche. These findings highlight the strong ability of KRT7 to modulate the TME. In our study, we employed a spontaneous orthotopic mouse model rather than a liver metastasis model induced by injection of cells into the spleen<sup>34,35</sup>. This choice was primarily motivated by the fact that the cellular composition of the spleen vastly differs from that of the pancreas, rendering it an inadequate mimic of the TME of primary pancreatic tumors<sup>34,35</sup>. Consistent with previous studies, we assessed liver metastatic potential as a clinically relevant measure of metastatic capability<sup>35,36</sup>. In both the BALB/c nude and C57BL/6 mouse models, KRT7 overexpression increased the incidence of liver metastasis without affecting tumor cell proliferation, which is consistent with the role of KRT7 in promoting metastasis through the modulation of CAFs rather than through direct effects on immune cells. These findings further improve our understanding of the mechanism by which KRT7 promotes PDAC liver metastasis, emphasizing that KRT7 influences the TME rather than directly impacting tumor cell proliferation.

Interestingly, when we studied the crosstalk between KRT7-expressing tumor cells and the TME, we found that the expression level of KRT7 was inversely correlated with the infiltration of CAFs in the TME, which is inconsistent from the well-known cancer-promoting effect of CAFs. This may also explain why the proliferation of primary tumor cells was not significantly affected, as it is often believed that CAFs promote tumor cell proliferation<sup>37</sup>. Moreover, we did not find any significant changes in the numbers of other antitumor immune cells, such as CD4<sup>+</sup> and CD8<sup>+</sup> T cells, as CAFs mainly suppress T-cell antitumor immunity<sup>38,39</sup>. When the infiltration of CAFs is reduced, CAFs do not exert pro-cancer effects but rather promote the occurrence of liver metastasis by reducing ECM deposition<sup>38</sup>. Therefore, tumor treatment strategies that deplete/inhibit CAFs should be used with caution. In addition to the induction of CAF infiltration, the ability of CAFs cocultured with KRT7-overexpressing cells to produce ECM was evaluated *in vitro*, and the results revealed the suppressive effects of FGF2 on CAF activity. However, CAF activity could be influenced by TME-related factors, such as cytokines or hypoxia, *in vivo*<sup>40</sup>. KRT7 was reported to upregulate immune checkpoints, including CD274, CD276, and CTCN1, which act as immunosuppressants by transmitting signals to suppress effector T cells, further affecting the function of immune cells expressing related receptors<sup>41,42</sup>. However, it is still unknown whether it can indirectly regulate CAFs by causing changes in cytokine levels or the oxygen levels in the TME through other cells<sup>43</sup>.

In tumors with high KRT7 expression, ECM deposition in the TME is decreased, and CAF proliferation is suppressed by FGF2. We found that FGF2 is a crucial mediator in this process, as it inhibits ECM production through the suppression of the Wnt/ $\beta$ -catenin pathway, which is consistent with the findings of Tian et al.<sup>24</sup>. *In vivo*, we chose to directly target FGF2 rather than directly activating Wnt/ $\beta$ -catenin signaling in CAFs because interfering with the Wnt/ $\beta$ -catenin signaling pathway may lead to broad effects beyond CAF inhibition, potentially resulting in tumor progression<sup>44,45</sup>. Here, the use of an FGF2 inhibitor did not result in a significant tumor-promoting effect, even if it potentially promoted CAF proliferation, making it a promising option for combination therapies for tumors. Furthermore, KRT7 promotes the transcription of FGF2, suggesting that targeting KRT7 within tumor cells is a potential therapeutic approach; however, future studies are necessary to precisely delineate its transcriptional activities. Unlike the well-known ECM condition regulator TGF-beta, KRT7 did not directly change its expression or secretion in PDAC to impact the ECM. It is possible that tumor-derived TGF-beta may not be necessary for the formation of a metastatic ECM niche. Furthermore, a positive correlation between MMPs and KRT7 mRNA expression has been reported in breast cancer, which reflects the potential complicated role of KRT7 in promoting tumor EMT<sup>32</sup>. However, the interactions between KRT7 and other EMT-related molecules in PDAC still needs to be investigated and confirmed in the future.

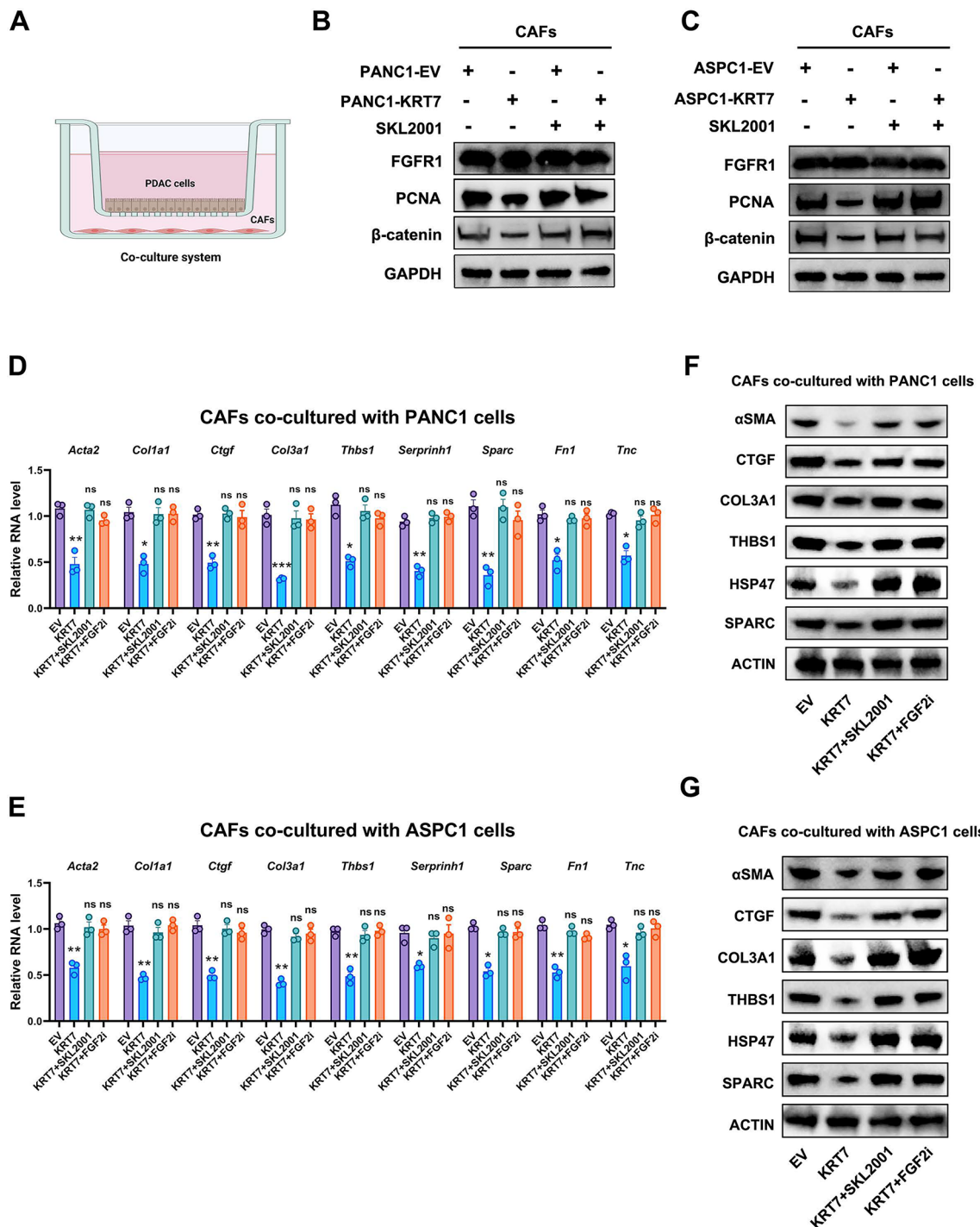


**Fig. 6.** FGF2 inhibits CAF proliferation and the transcription of ECM-related genes through the Wnt- $\beta$ -catenin signaling pathway. (A) Diagram of the indirect coculture system. (B,C) Western blot analysis of FGFR1, PCNA and  $\beta$ -catenin levels in cocultured CAFs (24 h) treated with or without SKL2001 (10  $\mu$ M). (D,E) RNA levels of ECM-related genes in cocultured CAFs (24 h) treated with SKL2001 (10  $\mu$ M) or NSC12 (1  $\mu$ M). (F,G) Representative protein levels of ECM-related genes in cocultured CAFs (24 h) treated with SKL2001 (10  $\mu$ M) or with NSC12 (1  $\mu$ M).

## Conclusion

In conclusion, this study revealed the pivotal role of KRT7 in triggering prometastatic niche formation to promote PDAC liver metastasis. KRT7 promotes FGF2 secretion by PDAC cells to inhibit CAF proliferation and decrease ECM deposition. These findings provide a basis for the clinical application of strategies that target FGF2 to inhibit PDAC liver metastasis.

## Data availability

All the data generated or analyzed during this study are included in the supplementary information files.

Received: 20 June 2024; Accepted: 20 December 2024

Published online: 26 February 2025

## References

- Siegel, R. L., Giaquinto, A. N. & Jemal, A. Cancer statistics, 2024. *CA Cancer J. Clin.* **74**, 12–49. <https://doi.org/10.3322/caac.21820> (2024).
- Liao, C.-Y. et al. Necroptosis enhances ‘don’t eat me’ signal and induces macrophage extracellular traps to promote pancreatic cancer liver metastasis. *Nat. Commun.* **15**, 6. <https://doi.org/10.1038/s41467-024-50450-6> (2024).
- Karras, P., Black, J. R. M., McGranahan, N. & Marine, J.-C. Decoding the interplay between genetic and non-genetic drivers of metastasis. *Nature* **629**, 543–554. <https://doi.org/10.1038/s41586-024-07302-6> (2024).
- Lambert, A. W., Pattiabiraman, D. R. & Weinberg, R. A. Emerging biological principles of metastasis. *Cell* **168**, 670–691. <https://doi.org/10.1016/j.cell.2016.11.037> (2017).
- Reymond, N., d’Águia, B. B. & Ridley, A. J. Crossing the endothelial barrier during metastasis. *Nat. Rev. Cancer* **13**, 858–870. <https://doi.org/10.1038/nrc3628> (2013).
- Zhang, T., Ren, Y., Yang, P., Wang, J. & Zhou, H. Cancer-associated fibroblasts in pancreatic ductal adenocarcinoma. *Cell Death Dis.* **13**, 1. <https://doi.org/10.1038/s41419-022-05351-1> (2022).
- Najafi, M., Farhood, B. & Mortezaee, K. Extracellular matrix (ECM) stiffness and degradation as cancer drivers. *J. Cell. Biochem.* **120**, 2782–2790. <https://doi.org/10.1002/jcb.27681> (2018).
- Sun, X. et al. Inflammatory cell-derived CXCL3 promotes pancreatic cancer metastasis through a novel myofibroblast-hijacked cancer escape mechanism. *Gut* **71**, 129–147. <https://doi.org/10.1136/gutjnl-2020-322744> (2022).
- Mao, X. et al. Crosstalk between cancer-associated fibroblasts and immune cells in the tumor microenvironment: New findings and future perspectives. *Mol. Cancer* **20**, 1. <https://doi.org/10.1186/s12943-021-01428-1> (2021).
- Murgai, M. et al. KLF4-dependent perivascular cell plasticity mediates pre-metastatic niche formation and metastasis. *Nat. Med.* **23**, 1176–1190. <https://doi.org/10.1038/nm.4400> (2017).
- Hosseinalizadeh, H. et al. Emerging insights into keratin 7 roles in tumor progression and metastasis of cancers. *Front. Oncol.* **13**, 871. <https://doi.org/10.3389/fonc.2023.1243871> (2024).
- Elazzezy, M. et al. Emerging insights into keratin 16 expression during metastatic progression of breast cancer. *Cancers* **13**, 869. <https://doi.org/10.3390/cancers13153869> (2021).
- Chen, S. et al. *Fusobacterium nucleatum* promotes colorectal cancer metastasis by modulating KRT7-AS/KRT7. *Gut Microbes* **11**, 511–525. <https://doi.org/10.1080/19490976.2019.1695494> (2020).
- Carotenuto, P. et al. Wnt signalling modulates transcribed-ultraconserved regions in hepatobiliary cancers. *Gut* **66**, 1268–1277. <https://doi.org/10.1136/gutjnl-2016-312278> (2017).
- Kang, F. P. et al. *Escherichia coli*-induced cGLIS3-mediated stress granules activate the NF-κB pathway to promote intrahepatic cholangiocarcinoma progression. *Adv. Sci.* **11**, 174. <https://doi.org/10.1002/advs.202306174> (2024).
- Wan Mohammad, W. M. Z. Sample size calculation in animal studies using resource equation approach. *Malays. J. Med. Sci.* **24**, 101–105. <https://doi.org/10.21315/mjms2017.24.5.11> (2017).
- Franco-Barraza, J., Beacham, D. A., Amatangelo, M. D. & Cukierman, E. Preparation of extracellular matrices produced by cultured and primary fibroblasts. *Curr. Protoc. Cell Biol.* **71**, 11–34. <https://doi.org/10.1002/cpcb.2> (2016).
- De Padilla, C. M. L. et al. Picosirius red staining: Revisiting its application to the qualitative and quantitative assessment of collagen type I and type III in tendon. *J. Histochem. Cytochem.* **69**, 633–643. <https://doi.org/10.1369/00221554211046777> (2021).
- Jiang, L. et al. Prospective observational study on biomarkers of response in pancreatic ductal adenocarcinoma. *Nat. Med.* **30**, 749–761. <https://doi.org/10.1038/s41591-023-02790-x> (2024).
- Moffitt, R. A. et al. Virtual microdissection identifies distinct tumor- and stroma-specific subtypes of pancreatic ductal adenocarcinoma. *Nat. Genet.* **47**, 1168–1178. <https://doi.org/10.1038/ng.3398> (2015).
- Yu, Y., Wang, Z., Mo, D. H., Wang, Z. & Li, G. Transcriptome profiling reveals liver metastasis-associated genes in pancreatic ductal adenocarcinoma. *Math. Biosci. Eng.* **18**, 1708–1721. <https://doi.org/10.3934/mbe.2021088> (2021).
- Tang, Z., Kang, B., Li, C., Chen, T. & Zhang, Z. GEPIA2: An enhanced web server for large-scale expression profiling and interactive analysis. *Nucleic Acids Res.* **47**, W556–W560. <https://doi.org/10.1093/nar/gkz430> (2019).
- Zeng, J. et al. CancerSCEM: A database of single-cell expression map across various human cancers. *Nucleic Acids Res.* **50**, D1147–D1155. <https://doi.org/10.1093/nar/gkab905> (2022).
- Tian, X. et al. Fibroblast growth factor 2 acts as an upstream regulator of inhibition of pulmonary fibroblast activation. *FEBS Open Bio* **13**, 1895–1909. <https://doi.org/10.1002/2211-5463.13691> (2023).
- Ronca, R. et al. Long-pentraxin 3 derivative as a small-molecule FGF trap for cancer therapy. *Cancer Cell* **28**, 225–239. <https://doi.org/10.1016/j.ccr.2015.07.002> (2015).
- Chen, X. et al. Inhibition of Wnt/beta-catenin signaling suppresses bleomycin-induced pulmonary fibrosis by attenuating the expression of TGF-β1 and FGF-2. *Exp. Mol. Pathol.* **101**, 22–30. <https://doi.org/10.1016/j.yexmp.2016.04.003> (2016).
- Gwak, J. et al. Small molecule-based disruption of the Axin/β-catenin protein complex regulates mesenchymal stem cell differentiation. *Cell Res.* **22**, 237–247. <https://doi.org/10.1038/cr.2011.127> (2011).
- Ohashi, W., Yamamine, N., Imura, J. & Hattori, Y. SKL2001 suppresses colon cancer spheroid growth through regulation of the E-cadherin/β-catenin complex. *Biochem. Biophys. Res. Commun.* **493**, 1342–1348. <https://doi.org/10.1016/j.bbrc.2017.09.161> (2017).
- Hwang, S.-Y. et al. Direct targeting of β-catenin by a small molecule stimulates proteasomal degradation and suppresses oncogenic Wnt/β-catenin signaling. *Cell Rep.* **16**, 28–36. <https://doi.org/10.1016/j.celrep.2016.05.071> (2016).
- Boyd, L. N. C., Andini, K. D., Peters, G. J., Kazemier, G. & Giovannetti, E. Heterogeneity and plasticity of cancer-associated fibroblasts in the pancreatic tumor microenvironment. *Semin. Cancer Biol.* **82**, 184–196. <https://doi.org/10.1016/j.semcan.2021.03.006> (2022).
- Zhang, C. et al. Identifying a baicalein-related prognostic signature contributes to prognosis prediction and tumor microenvironment of pancreatic cancer. *Front. Immunol.* **14**, 650. <https://doi.org/10.3389/fimmu.2023.1223650> (2023).
- Chen, F. et al. N6-Methyladenosine regulates mRNA stability and translation efficiency of KRT7 to promote breast cancer lung metastasis. *Cancer Res.* **81**, 2847–2860. <https://doi.org/10.1158/0008-5472.CAN-20-3779> (2021).
- Landau, M. S., Kuan, S.-F., Chiosea, S. & Pai, R. K. BRAF-mutated microsatellite stable colorectal carcinoma: An aggressive adenocarcinoma with reduced CDX2 and increased cytokeratin 7 immunohistochemical expression. *Hum. Pathol.* **45**, 1704–1712. <https://doi.org/10.1016/j.humpath.2014.04.008> (2014).
- Foley, K. et al. Semaphorin 3D autocrine signaling mediates the metastatic role of annexin A2 in pancreatic cancer. *Sci. Signal.* **8**, 823. <https://doi.org/10.1126/scisignal.aaa5823> (2015).
- Huang, C. et al. Tumour-derived interleukin 35 promotes pancreatic ductal adenocarcinoma cell extravasation and metastasis by inducing ICAM1 expression. *Nat. Commun.* **8**, 14035. <https://doi.org/10.1038/ncomms14035> (2017).

36. Garcia Garcia, C. J. et al. Stromal HIF2 regulates immune suppression in the pancreatic cancer microenvironment. *Gastroenterology* **162**, 2018–2031. <https://doi.org/10.1053/j.gastro.2022.02.024> (2022).
37. Geng, X. et al. Cancer-associated fibroblast (CAF) heterogeneity and targeting therapy of CAFs in pancreatic cancer. *Front. Cell Dev. Biol.* **9**, 152. <https://doi.org/10.3389/fcell.2021.655152> (2021).
38. Tsoumakidou, M. The advent of immune stimulating CAFs in cancer. *Nat. Rev. Cancer* **23**, 258–269. <https://doi.org/10.1038/s41568-023-00549-7> (2023).
39. Chen, Y. et al. Epithelial cells activate fibroblasts to promote esophageal cancer development. *Cancer Cell* **41**, 903–918. <https://doi.org/10.1016/j.ccr.2023.03.001> (2023).
40. Fang, Z. et al. Signaling pathways in cancer-associated fibroblasts: Recent advances and future perspectives. *Cancer Commun.* **43**, 3–41. <https://doi.org/10.1002/cac2.12392> (2022).
41. Li, Y., Su, Z., Wei, B. & Liang, Z. KRT7 overexpression is associated with poor prognosis and immune cell infiltration in patients with pancreatic adenocarcinoma. *Int. J. Gen. Med.* **4**, 2677–2694. <https://doi.org/10.2147/ijgm.S313584> (2021).
42. Chen, Y. et al. S100A2 is a prognostic biomarker involved in immune infiltration and predict immunotherapy response in pancreatic cancer. *Front. Immunol.* **12**, 4. <https://doi.org/10.3389/fimmu.2021.758004> (2021).
43. Hosseinalizadeh, H., Rahmati, M., Ebrahimi, A. & O'Connor, R. S. Current status and challenges of vaccination therapy for glioblastoma. *Mol. Cancer Therap.* **22**, 435–446. <https://doi.org/10.1158/1535-7163.Mct-22-0503> (2023).
44. Liu, J. et al. Wnt/β-catenin signalling: Function, biological mechanisms, and therapeutic opportunities. *Signal Transduct. Target. Ther.* **7**, 6. <https://doi.org/10.1038/s41392-021-00762-6> (2022).
45. Yu, F. et al. Wnt/β-catenin signaling in cancers and targeted therapies. *Signal Transduct. Target. Ther.* **6**, 5. <https://doi.org/10.1038/s41392-021-00701-5> (2021).

## Acknowledgements

This study was supported by the Startup Fund for Scientific Research, Fujian Medical University (Grant No. 2022QH1292 to Yuting Jiang), the Grant from Fujian Provincial Health Commission (No. 2020QNA004 to Jianlin Lai), and the National Natural Science Foundation of China (Grant No. 62375104 to Xiaoling Zheng), and the Provincial Hospital Affiliated with Fuzhou University National Natural Science Foundation Talent Cultivation Program (Grant No. 00802732 to Chengyu Liao).

## Author contributions

(I) Conception and design: Yuting Jiang, Chengyu Liao and Xiaoling Zheng; (II) administrative support: Xiaoling Zheng, Jianlin Lai; (III) provision of study materials or patients: Yuting Jiang, Chengyu Liao and Xiaoling Zheng; (IV) collection and assembly of data: Yunyi Peng, Qilin Chen; (V) data analysis and interpretation: Yuting Jiang, Chengyu Liao; (VI) manuscript writing: Yuting Jiang, Chengyu Liao; (VII) final approval of the manuscript: Xiaoling Zheng.

## Declarations

### Competing interests

The authors declare no competing interests.

### Ethical approval

All clinical tissue samples were obtained from Fujian Provincial Hospital, and this study was approved and authorized by the Ethics Committee of Fujian Provincial Hospital (K2024-06-034). All animal protocols and experiments were approved by the Institutional Animal Care and Use Committee (IACUC) of Fujian Anburui Biotechnology Co., Ltd. (IACUC FJABR2023080101) and were performed in accordance with the Guidelines for the Care and Use of Laboratory Animals.

### Additional information

**Supplementary Information** The online version contains supplementary material available at <https://doi.org/10.1038/s41598-024-84129-1>.

**Correspondence** and requests for materials should be addressed to C.L. or X.Z.

**Reprints and permissions information** is available at [www.nature.com/reprints](http://www.nature.com/reprints).

**Publisher's note** Springer Nature remains neutral with regard to jurisdictional claims in published maps and institutional affiliations.

**Open Access** This article is licensed under a Creative Commons Attribution-NonCommercial-NoDerivatives 4.0 International License, which permits any non-commercial use, sharing, distribution and reproduction in any medium or format, as long as you give appropriate credit to the original author(s) and the source, provide a link to the Creative Commons licence, and indicate if you modified the licensed material. You do not have permission under this licence to share adapted material derived from this article or parts of it. The images or other third party material in this article are included in the article's Creative Commons licence, unless indicated otherwise in a credit line to the material. If material is not included in the article's Creative Commons licence and your intended use is not permitted by statutory regulation or exceeds the permitted use, you will need to obtain permission directly from the copyright holder. To view a copy of this licence, visit <http://creativecommons.org/licenses/by-nc-nd/4.0/>.

© The Author(s) 2025